Analysis of DC-Link Operation Voltage of a Hybrid Railway Power Quality Conditioner and Its PQ Compensation Capability in High-Speed Cophase Traction Power Supply

Keng-Weng Lao, *Student Member, IEEE*, Man-Chung Wong, *Senior Member, IEEE*, Ning Yi Dai, *Member, IEEE*, Chi-Kong Wong, *Member, IEEE*, and Chi-Seng Lam, *Member, IEEE*

***Abstract*—Hybrid Railway Power Quality Conditioner (HPQC) is newly proposed for its effective reduction in dc-link operation voltage while providing similar power quality compensation in cophase traction power supply compared to conventional railway power quality conditioner. However, reduction in HPQC operation voltage limits its power quality compensation capability. For instance, the previously proposed HPQC design based on minimum operation voltage under fixed rated load has minimum power quality compensation capability. Under practical conditions when load varies, the required HPQC active and reactive compensation power also changes. The dc-link operation voltage of HPQC may therefore need to be enhanced to increase its power quality compensation capability. Therefore in this paper, the relationship between dc-link voltage of HPQC and its power quality compensation capability, as well as its limitations, are being analyzed. Simulation and experimental results are also presented to verify the mentioned relationship via investigations of system performance under different loading conditions. The research can provide a guideline for determination of HPQC operation voltage when load varies.**

***Index Terms*—Compensation capability, cophase power system, high-speed railway, hybrid railway power quality conditioner (HPQC), power quality.**

I. Introduction

WITH rapid country and city development around the world, electric railway transportation has played an essential role in economics and daily lives. This causes high and increasing transportation demand. It is therefore important that traction power supply is stable and can provide power with high power quality to locomotives. However, traction power supply usually suffers from various power quality problems such as reactive power, system unbalance, and harmonics, etc. [1]–[3]. Concerning these power quality problems, the Institute of Electrical and Electronics Engineers (IEEE) and Standardization Administration of the People's Republic of China have released corresponding tolerance standards [4], [5]. Various power quality compensation techniques, which are discussed in later sections, are therefore proposed.

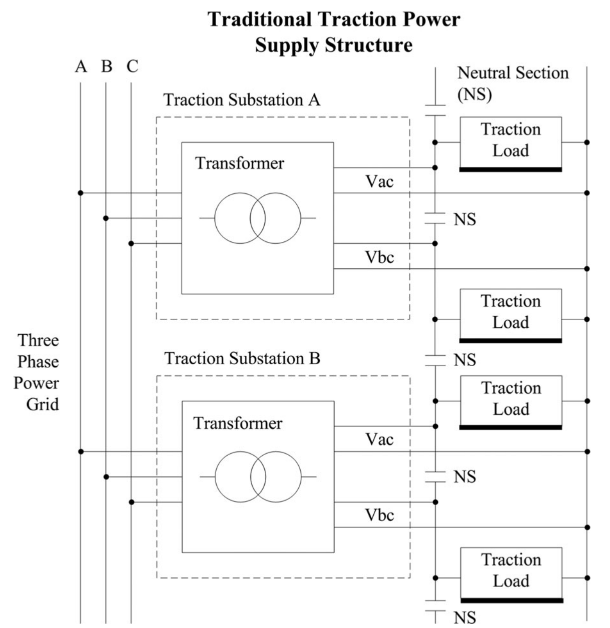

Fig. 1. Traditional power supply structure with NS to avoid phase mixing.

Nowadays, ac electrified power with 50 Hz, 25 kV is commonly used in long distance high-speed railway [3]. In traditional ac traction power supply (see Fig. 1), the power in three phase grid is transformed into two single phase outputs through substation and supply power to locomotives [6]. Since the two single phase power is of different phase, neutral sections (NSs) (without power supply) are required to avoid risk of phase mixing. As locomotives run through NSs, they lose power and velocity. Traditional ac power structure is therefore not suitable for high-speed railway. Based on this consideration, the cophase traction power supply system is proposed. In cophase traction power (see Fig. 2), locomotive loadings are connected across

Manuscript received November 3, 2014; revised February 8, 2015; accepted March 14, 2015. Date of publication March 26, 2015; date of current version September 29, 2015. This work was supported by the Science and Technology Development Fund (Project Code: 015/2008/A1), Macao SAR Government and the University of Macau Research Committee (Project Code: UL015/08-Y2/EEE/WMC01/FST), and the University of Macau Power Electronics Lab. Recommended for publication by Associate Editor S. K. Mazumder.

K.-W. Lao, N. Y. Dai, and C.-K. Wong are with the Department of Electrical and Computer Engineering, Faculty of Science and Technology, University of Macau, Macao 999078, China (e-mail: yb17424@umac.mo; nydai@umac.mo; ckwong@umac.mo).

M.-C. Wong and C.-S. Lam are with the Department of Electrical and Computer Engineering, Faculty of Science and Technology and State Key Laboratory of Analog and Mixed Signal VLSI, University of Macau, Macao 853, China (e-mail: mcwong@umac.mo; cslam@umac.mo).

Color versions of one or more of the figures in this paper are available online at http://ieeexplore.ieee.org.

Digital Object Identifier 10.1109/TPEL.2015.2417356

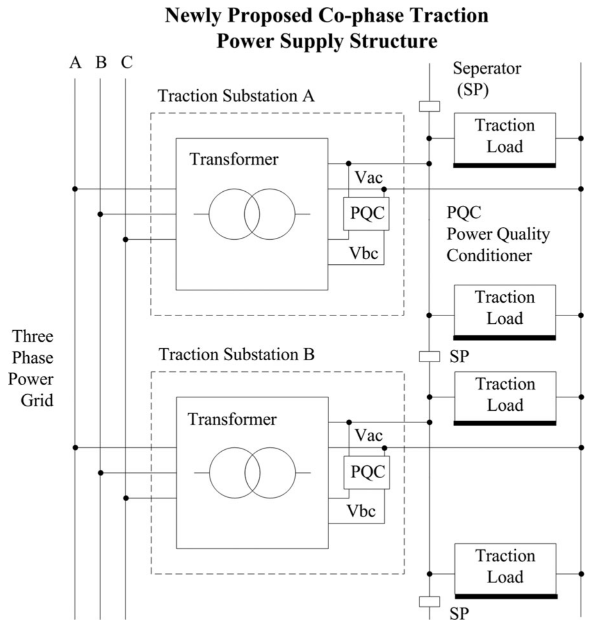

Fig. 2. Newly proposed cophase traction power supply structure.

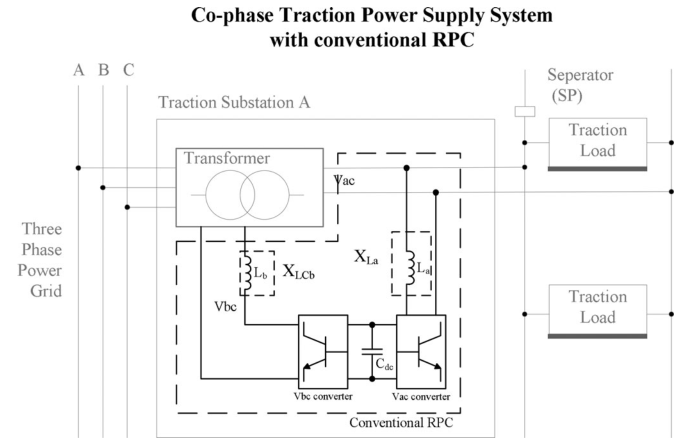

Fig. 3. Cophase traction power supply system with conventional inductive coupled RPC.

one single phase output of substation transformer only, leaving another phase unloaded. This proposed structure is beneficial for effective reduction of NSs and higher transformer utilization ratio. The cophase structure is thus more suitable for application in high-speed railway.

The idea of cophase traction power first appeared in [7] in year 2009. More details about hardware prototype and testing results of cophase traction power supply can be found in [8]. The world's first cophase traction power supply device has already be implemented and put into trial operation at MeiShan Substation of the Chengdu-Kunming Railway in 2012 in China. More details are presented in [9] and [10]. Cophase traction power supply system can balance three-phase traction power, and at the same time provide reactive power and harmonic compensation. Cophase traction power is also one of the important projects supported by the National Science and Technology Pillar Program during the 11th Five-Year Plan Period of China. These show the importance of cophase traction power in railway development.

As discussed, power quality issues are great concerns in traction power supply system. In order to achieve high power quality that can satisfy the IEEE and other standards, various power quality compensation techniques have been developed [11], [12]. Conventionally, passive compensators are used. For example, shunt capacitive bank is used to provide reactive power compensation for inductive traction load [13]. However, it can only provide fixed compensation capacity and cannot provide dynamic performance. Afterward, compensators based on active components are proposed. For instance, static var compensator is used [14], [15], but it cannot compensate system unbalance problem, and inject harmonics into the system. For system unbalance problem, although techniques such as installation of balance transformers or changing phase connection can be used, they cannot provide complete and unified compensation. In contrast, compensators based on active components can provide better dynamic performance. [16], [17] The railway power quality conditioner (RPC) is thus developed [18], [19]. It is widely adopted as a unified solution for reactive power, system unbalance and harmonics in traction power supply. Specially, in Europe, some traction locomotives are electrified with 15 kV, 16 2/3Hz other than system line frequency (usually of 50 Hz or 60 Hz). There are thus more on-going researches on the development of power electronic traction transformer (PETT) for improved efficiency and power conditioning, especially in Europe [20]–[22]. Field testing of PETT prototype has also been done with Swiss Federal Railways, and the system performance is satisfactory and has shown improvements. However, further investigations of PETT are required when traction locomotives are directly powered from system line utility grid, like in China, in which three-phase balancing is also concerned. RPC may be more suitable under this case.

A typical structure of RPC is shown in Fig. 3. It is basically composed of a back to back converter with a common dc link. One converter, for instance, the V_{ac} phase converter is connected to the locomotive phase through inductive coupled impedance; and another phase, V_{bc} phase converter, is connected to the unloaded phase through inductive coupled impedance. In order to control the power flow so as to achieve power quality compensation, the energy of the dc link must be higher than the point of common coupling (PCC) point. In other words, the dc-link voltage must be higher than the peak of V_{ac} voltage. This induces high dc-link voltage requirement in traditional RPC. The device rating and power loss, as well as the cost, are therefore higher. Hybrid railway power quality conditioner (HPQC) in Fig. 4 is thus proposed and developed. Different from traditional RPC, the V_{ac} phase converter in HPQC is connected to the PCC through capacitive coupled impedance. The capacitive coupled capacitance can help to provide support voltage during reactive power compensation so that the dc-link voltage can be decreased. The device rating and cost of HPQC can thus be reduced.

The idea of HPQC is first proposed in [23] in year 2012. More details and derivations of system parameter design can be found

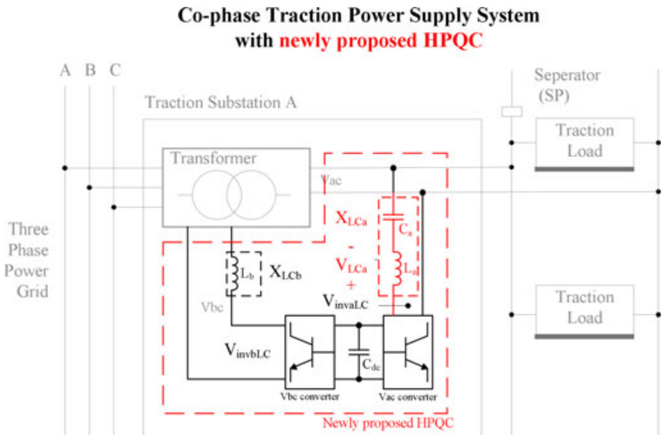

Fig. 4. Cophase traction power supply system with the proposed capacitive coupled HPQC.

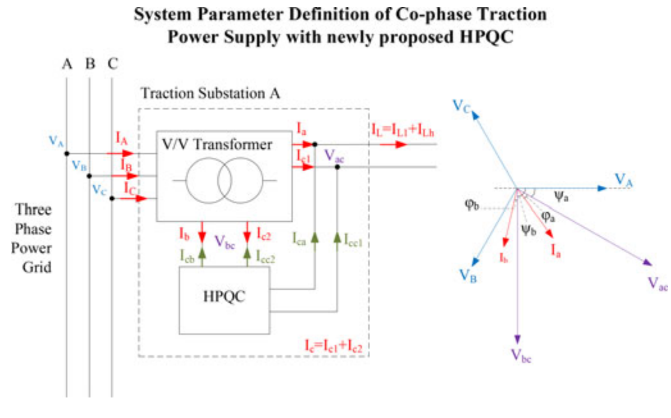

Fig. 5. Circuit schematics and vector diagram which show parameter definition of cophase traction power supply with newly proposed HPQC.

in [24] and [25]. A brief review of voltage reduction mechanism in HPQC is also covered in the next section. However, the HPQC is designed based on the criteria of minimum operation voltage requirement under fixed rated load. Under minimum operation voltage, the HPQC compensation capability is limited and minimized. In other words, the HPQC can provide satisfactory compensation performance only at the designed fixed rated load. The HPQC power quality compensation capability is somehow limited by reduction in operation voltage.

The operation voltage of power compensators may be enhanced to provide satisfactory performance for wider range of loadings [26], [27]. Therefore, under practical conditions when traction load varies, the required active and reactive compensation power from HPQC also changes, the dc-link voltage of HPQC may then need to be increased. However, the HPQC dc-link voltage requirement is not directly proportional and does not vary linearly with load variations. Furthermore, load variations include both variations in load power factor and capacity. Therefore, it is important and worthy to investigate the relationship between HPQC dc-link voltage and its power quality compensation capability in cophase traction power.

In this paper, the relationship between HPQC dc-link operation voltage and its compensation capability is analyzed and discussed so as to provide a guideline for determination of HPQC dc-link voltage when load varies. In Section I, a brief introduction of research background and motivation is covered. In Section II, the HPQC control algorithm and design based on minimum operation voltage at rated load is reviewed. The relationship between HPQC compensation capability and dc-link voltage, as well as their limitations, are then analyzed and discussed in Section III. In Section IV, simulation verifications and experimental results obtained from hardware prototype are presented. Finally, a conclusion is given in Section V.

II. HPQC Compensation Algorithm and Minimum DC-Link Operation Voltage Design

The HPQC compensation algorithm details can be found in [23] and [24]. The analysis that follows is developed based on the control algorithm. The core algorithm shown in (1) is used for determination of HPQC $\mathrm{V_{ac}}$ phase converter active (p_{ca}) and reactive (q_{ca}) power, as well as $\mathrm{V_{bc}}$ phase converter active (p_{cb}) and reactive (q_{cb}) power. $\bar{p}_L$ and $\tilde{p}_L$ refer to the dc and ac components of load active (real) power, respectively; while $\mathrm{q_L}$ refers to the reactive (imaginary) power. This core equation is derived based on the system power quality requirement model (ideal compensation). System compensation is provided from the transformer secondary side (refer to Fig. 4). It is shown through the equation that in order to maintain a balanced system, half of the load active power is transferred from $\mathrm{V_{bc}}$ phase to $\mathrm{V_{ac}}$ phase converter; the system source reactive power problem is then compensated by transferring appropriate amount of reactive power between the two phases. Finally, the load reactive power is compensated by the $\mathrm{V_{ac}}$ phase converter

$$\begin{bmatrix} p_{ca} \\ q_{ca} \\ p_{cb} \\ q_{cb} \end{bmatrix} = \begin{bmatrix} \frac{1}{2}\bar{p}_L + \tilde{p}_L \\ \frac{1}{2\sqrt{3}}\bar{p}_L + q_L \\ -\frac{1}{2}\bar{p}_L \\ -\frac{1}{2\sqrt{3}}\bar{p}_L \end{bmatrix}. \tag{1}$$

As described in [24], the HPQC operation voltage is dominant by the $\mathrm{V_{ac}}$ phase converter; therefore, the $\mathrm{V_{bc}}$ phase converter operation voltage will not be discussed in the analysis.

Some parameter definitions of system voltage and current are presented in Fig. 5. The parameters for HPQC analysis are also defined in Fig. 4. The capacitive coupled impedance of $\mathrm{V_{ac}}$ phase is X_{LCa}, and the $\mathrm{V_{ac}}$ phase inverter output voltage is V_{invaLC}. Furthermore, the voltage drop across the coupled impedance X_{LCa} is defined as V_{LCa}; and the phase angle between V_{ac} and I_{ca} is θ_{ca}.

The vector diagram showing the operation of HPQC $\mathrm{V_{ac}}$ phase converter under minimum operation voltage is given in Fig. 6.

With capacitive coupled impedance X_{LCa}, the vector V_{LCa} is always 90° clockwise with the vector I_{ca}. Under fixed load, the amplitude I_{ca} is also fixed; as X_{LCa} varies, the length of V_{LCa} varies along the line L_1. Moreover, the relationship in (2) can be derived from circuit analysis

$$\vec{V}_{\mathrm{invaLC}} = \vec{V}_{\mathrm{ac}} + \vec{V}_{\mathrm{LC}a}. \tag{2}$$

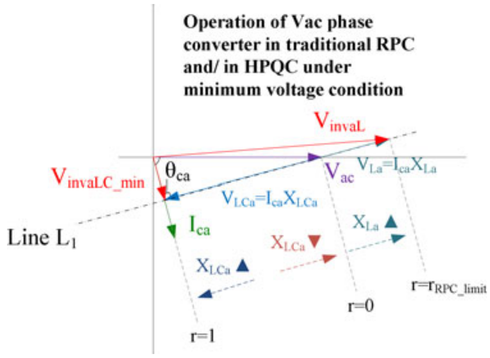

Fig. 6. Vector diagram showing V_{ac} phase converter operation in traditional RPC and in HPQC under minimum operation voltage.

On the other hand, with inductive coupled impedance X_{La} (in traditional RPC), the vector V_{La} is always 90° anticlockwise with the vector $I_{\rm ca}$, such that the relationship in (3) can be derived

$$\vec{V}_{\mathrm{inva}L} = \vec{V}_{\mathrm{ac}} + \vec{V}_{La}. \tag{3}$$

It is worth noticed that the value of dc-link voltage $V_{\rm DC}$ is a multiple of square root two times of $V_{\rm invaLC}$ as shown in (4). Minimization of HPQC dc-link voltage thus also refers to minimization of $V_{\rm invaLC}$

$$V_{\mathrm{DC}} = \sqrt{2} \cdot V_{\mathrm{invaLC}}. \tag{4}$$

With fixed load condition, $I_{\rm ca}$ is fixed; with proposed HPQC, as $X_{\rm LCa}$ increases, the magnitude of $V_{\mathrm{LC}a}$ also increases; on the other hand, as $X_{\mathrm{LC}a}$ decreases, the magnitude of $V_{\mathrm{LC}a}$ also decreases. From Fig. 6 and (2), one can observe that the magnitude of $V_{\rm invaLC}$ can alter be altered by the magnitude of $V_{\mathrm{LC}a}$. Therefore, an optimized value of $V_{\rm invaLC}$ can be achieved with a proper selection of $X_{\mathrm{LC}a}$. It can also be inferred from Fig. 6 that the amplitude of $V_{\rm invaLC}$ is minimized when $V_{\rm invaLC}$ is perpendicular with the line L_1. Under this minimized condition, the amplitude of $V_{\mathrm{LC}a}$ satisfies the expression in (5). Notice that the subscript "rated" refers to parameters at rated design

$$\begin{aligned} \left|\vec{V}_{\mathrm{LC}a\_\mathrm{rated}}\right| &= \left|\vec{V}_{\mathrm{ac}}\right| \cdot \sin\theta_{ca\_\mathrm{rated}} \\ &= (I_{ca\_\mathrm{rated}}) \cdot (X_{\mathrm{LC}a\_\mathrm{rated}}). \end{aligned} \tag{5}$$

Therefore, the value of $X_{\mathrm{LC}a}$ can be selected by (6), after further manipulation of (5), for minimum HPQC dc-link operation voltage at rated condition

$$X_{\mathrm{LC}a\_\mathrm{rated}} = \frac{V_{\mathrm{ac}} \sin\theta_{ca\_\mathrm{rated}}}{I_{ca\_\mathrm{rated}}}. \tag{6}$$

The value of $\theta_{\rm ca}$, known as the $V_{\rm ac}$ phase compensation angle, can be determined by (7), which is derived from (1)

$$\begin{aligned} \theta_{ca} &= \tan^{-1}\left[\frac{\frac{1}{2\sqrt{3}}(\mathrm{PF}_L) + \sin\left(\cos^{-1}(\mathrm{PF}_L)\right)}{\frac{1}{2}(\mathrm{PF}_L)}\right] \\ &= \tan^{-1}\left[\frac{\frac{1}{2\sqrt{3}}(\mathrm{PF}_L) + \sqrt{1-(\mathrm{PF}_L)^2}}{\frac{1}{2}(\mathrm{PF}_L)}\right]. \end{aligned} \tag{7}$$

The minimum HPQC operation voltage, which is also the minimum amplitude of $V_{\rm invaLC}$, can therefore be determined by (8)

$$V_{\mathrm{invaLC\_min}} = V_{\mathrm{ac}} \cdot \cos\theta_{ca\_\mathrm{rated}}. \tag{8}$$

For comparison, similar analysis is performed on conventional RPC. Similarly, as X_{La} increases, the amplitude of V_{La} increases toward the right-hand side of Fig. 6, and vice versa. According to Fig. 6 and (3), with fixed load capacity and compensation current $I_{\rm ca}$, the amplitude of V_{La} and required operation voltage $V_{\rm invaL}$ increases as coupled impedance X_{La} increases. However, unlike newly proposed HPQC, there is no impedance design such that operation voltage in traditional RPC, $V_{\rm invaL}$ can be minimized at rated design. Instead, the value of $V_{\rm invaL}$ is directly determined by the compensation current $I_{\rm ca}$ and coupled impedance X_{La}, as represented in (9)

$$|V_{\mathrm{invaL}}| = \sqrt{(I_{ca}X_{La}\cos\theta_{ca})^2 + (V_{\mathrm{ac}} + I_{ca}X_{La}\sin\theta_{ca})^2}. \tag{9}$$

Since load capacity variation is involved in further analysis, the load capacity can be considered to be varying with r, in which r is expressed as per unit value for load capacity. For instance, at rated load capacity, *r* equals 1. With fixed $X_{\mathrm{LC}a}$, the magnitude of $V_{\mathrm{LC}a}$ will also be changed when r changes. When $r = 0$, the magnitude of $V_{\mathrm{LC}a}$ is the smallest. On the other hand, in traditional RPC, the range of loading that can be compensated is limited by the value of $r_{\mathrm{RPC\_limit}}$, which can be determined using (10) shown at the bottom of the page, obtained through further manipulation of (9). These are also illustrated in Fig. 6:

III. Analysis of RPC and HPQC DC-Link Voltage and Compensation Capability

When the HPQC is designed based on minimum dc-link operation voltage, the compensation capability is minimized. Under practical conditions when load varies, the HPQC dc-link operation voltage may need to be enhanced to increase the compensation capability. In conventional RPC, this is accomplished by increasing its operation voltage over the PCC voltage $V_{\rm ac}$. More details are discussed next.

Shown in Fig. 7 is a vector diagram showing the RPC and HPQC operation with enhanced operation voltage under variations in loading conditions. It also shows the relationship

$$r_{\mathrm{RPC\_limit}} = \frac{-\left(2V_{\mathrm{ac}}I_{ca\_\mathrm{rated}}X_{La}\sin\theta_{ca}\right) + \sqrt{\left(2V_{\mathrm{ac}}I_{ca\_\mathrm{rated}}\sin\theta_{ca}\right)^2 - 4\left(I_{ca\_\mathrm{rated}}X_{La}\right)^2\left(V_{\mathrm{ac}}^2 - V_{\mathrm{invaL}}^2\right)}}{2\left(I_{ca\_\mathrm{rated}}X_{La}\right)^2} \tag{10}$$

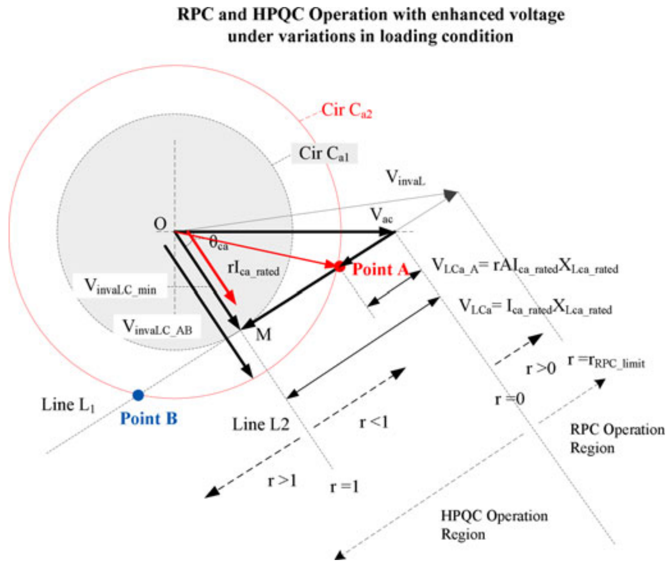

Fig. 7. Vector diagram showing the operation of RPC and HPQC with enhanced operation voltage under variations in loading conditions.

between HPQC operation voltage V_{invaLC} and the power quality compensation capability. It is assumed that as traction load capacity varies, the $\mathrm{V_{ac}}$ phase compensation current is changed to *r* times of rated value, $rI_{\mathrm{ca\_rated}}$.

A. RPC Compensation Capability With Operation Voltage Over PCC Voltage

As discussed previously and observed from Figs. 6 and 7, the RPC operation voltage must be larger than PCC voltage V_{ac} in order to provide satisfactory compensation for inductive traction load. The RPC compensation capability is restricted by (10). When load capacity ratio *r* increases, the value of required operation voltage V_{invaL} also increases, and vice versa. Although compensation may be provided from 0 to $r_{\mathrm{RPC\_limit}}$ in traditional RPC, the design is less practical since high operation voltage is required and RPC disconnection is preferred under no-load case.

B. HPQC Compensation Capability at Rated Design Under Minimum Operation Voltage

With rated load capacity, $r = 1$, the value of $X_{\mathrm{LC}a}$ is selected according to (6) such that V_{invaLC} is perpendicular with $V_{\mathrm{LC}a}$. With this minimum HPQC operation voltage, the compensation region is bounded by the circle with radius $V_{\mathrm{invaLC\_min}}$, as indicated by the shaded area within the circle Cir C_{a1} in Fig. 7. At rated load ($r = 1$), the edge of $V_{\mathrm{LC}a}$ is located at the boundary of the circle Cir C_{a1} (compensation region), HPQC can thus provide satisfactory compensation. However, as traction load capacity r differs from rated load ($r > 1$, or $r < 1$), the edge of $V_{\mathrm{LC}a}$ will be located outside the circle Cir C_{a1} at which HPQC cannot provide satisfactory compensation performance. Therefore, with minimum HPQC dc-link voltage, the power quality compensation capability is limited at rated load ($r = 1$).

C. Enhanced HPQC Compensation Capability With Operation Voltage Over Minimum Value

The minimum HPQC operation voltage which has minimum HPQC compensation capability can be determined by (8). In order to enhance the HPQC compensation capability, the operation voltage can be increased to $V_{\mathrm{invaLC\_AB}}$ as shown in Fig. 7. It can be seen that the compensation region is increased to the area bounded by the outermost circle Cir C_{a2}, with radius of $V_{\mathrm{invaLC\_AB}}$.

The relationship of $V_{\mathrm{invaLC\_AB}}$ in Fig. 7 can then be expressed mathematically as shown in (11). When the HPQC operation voltage is increased to $V_{\mathrm{invaLC\_AB}}$, there are different values of I_{cap} and I_{caq} that can satisfy the expression. In cophase traction power, the changes of I_{cap} and I_{caq} are restricted by (1) according to the load condition. Therefore, when the HPQC operation voltage is enhanced, the power quality compensation capability can be increased, and provide satisfactory compensation for a range of loading conditions

$$|V_{\mathrm{invaLC\_AB}}| \geq \sqrt{(V_{\mathrm{ac}} - |I_{\mathrm{caq}}| \cdot |X_{\mathrm{LC}a\mathrm{\_rated}}|)^2 + (|I_{\mathrm{cap}}| \cdot |X_{\mathrm{LC}a\mathrm{\_rated}}|)^2}. \tag{11}$$

By substituting (6) into (11), the expression in (12) shown at the bottom of the page, can be obtained. In order to simplify the analysis, the amplitude of V_{ac} is assumed to be fixed in the system, the equation in (12) is divided by V_{ac} to obtain the parameter, defined as the HPQC operation voltage rating, k_{invaLC}, as presented in (13) shown at the bottom of the page.

Furthermore, it is also assumed that as traction load varies, load variations do not only vary in load capacity (*r*), but also in load power factor (PF_L). Notice from (7) that θ_{ca} changes with different load power factor PF_L and therefore can be used to model load variations. Assuming that the required $\mathrm{V_{ac}}$ phase active and reactive power changes as shown in (14) and (15), the ratio of $\cos\theta_{\mathrm{ca}}$ to $cos\theta_{ca_{\mathrm{rated}}}$ is defined as h_c, and the ratio

$$|V_{\mathrm{invaLC\_AB}}| \geq \sqrt{\left(V_{\mathrm{ac}} - |I_{caq}| \cdot \left(\frac{V_{\mathrm{ac}} \sin\theta_{ca\_\mathrm{rated}}}{I_{ca\_\mathrm{rated}}}\right)\right)^2 + \left(|I_{\mathrm{cap}}| \cdot \left(\frac{V_{\mathrm{ac}} \cos\theta_{ca\_\mathrm{rated}}}{I_{ca\_\mathrm{rated}}}\right)\right)^2} \tag{12}$$

$$k_{\mathrm{invaLC\_AB}} = \frac{|V_{\mathrm{invaLC\_AB}}|}{V_{\mathrm{ac}}} \geq \sqrt{\left(1 - |I_{\mathrm{caq}}| \cdot \left(\frac{\sin\theta_{ca\_\mathrm{rated}}}{I_{ca\_\mathrm{rated}}}\right)\right)^2 + \left(|I_{\mathrm{cap}}| \cdot \left(\frac{\cos\theta_{ca\_\mathrm{rated}}}{I_{ca\_\mathrm{rated}}}\right)\right)^2} \tag{13}$$

of $\sin\theta_{\rm ca}$ to $\sin\theta_{ca\_{\rm rated}}$ is defined as h_s

$$\frac{p_{ca}}{p_{ca\_{\rm rated}}} = \frac{r\cdot(I_{ca\_{\rm rated}})\cdot(\cos\theta_{ca})}{(I_{ca\_{\rm rated}})\cdot(\cos\theta_{ca\_{\rm rated}})} = r\cdot\left(\frac{\cos\theta_{ca}}{\cos\theta_{ca\_{\rm rated}}}\right) = r\cdot h_c \tag{14}$$

$$\frac{q_{ca}}{q_{ca\_{\rm rated}}} = \frac{r\cdot(I_{ca\_{\rm rated}})\cdot(\sin\theta_{ca})}{(I_{ca\_{\rm rated}})\cdot(\sin\theta_{ca\_{\rm rated}})} = r\cdot\left(\frac{\sin\theta_{ca}}{\sin\theta_{ca\_{\rm rated}}}\right) = r\cdot h_s. \tag{15}$$

When the parameters r, h_s, and h_c are included, the expressions of $I_{\rm cap}$ and $I_{\rm caq}$ can be manipulated as (16)

$$\begin{cases} I_{\rm cap} = r\cdot I_{ca\_{\rm rated}}\cdot h_c\cdot\cos\theta_{ca\_{\rm rated}} \\ I_{\rm caq} = r\cdot I_{ca\_{\rm rated}}\cdot h_s\cdot\sin\theta_{ca\_{\rm rated}}. \end{cases} \tag{16}$$

The HPQC operation voltage rating can then be determined by substituting (16) into (13) as

The solutions of r for (17) shown at the bottom of the page, then signify the intersection points of the line L_1 and the circle Cir C_{a2} in Fig. 7 under HPQC operation voltage $V_{\rm invaLC\_AB}$. The results are shown in (18). Notice that h_c is also expressed as a function of h_s during manipulations since referring to (14) and (15), $(h_s)^2 + (h_c)^2 = 1$. The middle point of the loading range is denoted as r_M and is shown as follows:

$$\begin{cases} r_A \le r \le r_B \\ r_A = h_s - \sqrt{(h_s)^2 - \frac{1-(k_{\rm invaLC\_AB})^2}{(\sin\theta_{ca\_{\rm rated}})^2}} = h_s - \Delta \\ r_B = h_s + \sqrt{(h_s)^2 - \frac{1-(k_{\rm invaLC\_AB})^2}{(\sin\theta_{ca\_{\rm rated}})^2}} = h_s + \Delta \\ r_M = \frac{r_A + r_B}{2} = h_s. \end{cases} \tag{18}$$

For instance, traction load power factor mostly ranges from 0.8 to 0.9 [28]. Supposing that the HPQC is designed at rated load power factor 0.85, the HPQC compensation capability is plotted in Fig. 8 according to (17).

The minimum HPQC operation voltage rating calculated using (8) is 0.48. For example, when HPQC operation voltage rating is increased to 0.66, the intersection points between the horizontal line $k_{\rm invaLC\_AB} = 0.66$ and the curves then indicate the boundaries of the load capacity rating within the HPQC compensation capability under different traction load power factor.

The lower r value refers to point A (r_A) and the higher one refers to point B (r_B) in Fig. 7 above and Fig. 9 below. The middle point r_M is also indicated in the figure. The expressions for determination of $r_{A,}$, r_B and r_M can be found in (18). The followings can be observed from Fig. 8.

1) As long as the HPQC operation voltage is higher than its minimum value, it can always provide satisfactory compensation performance at rated condition.

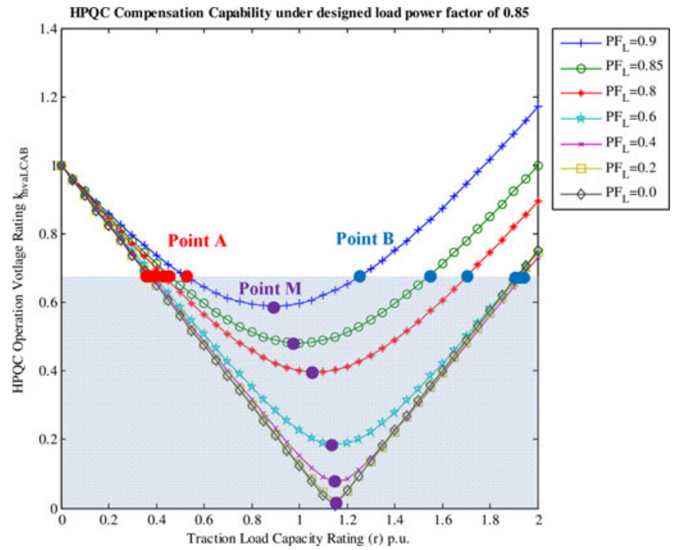

Fig. 8. MATLAB plot showing the HPQC compensation capability when load power factor varies (HPQC designed based on rated load power factor of 0.85).

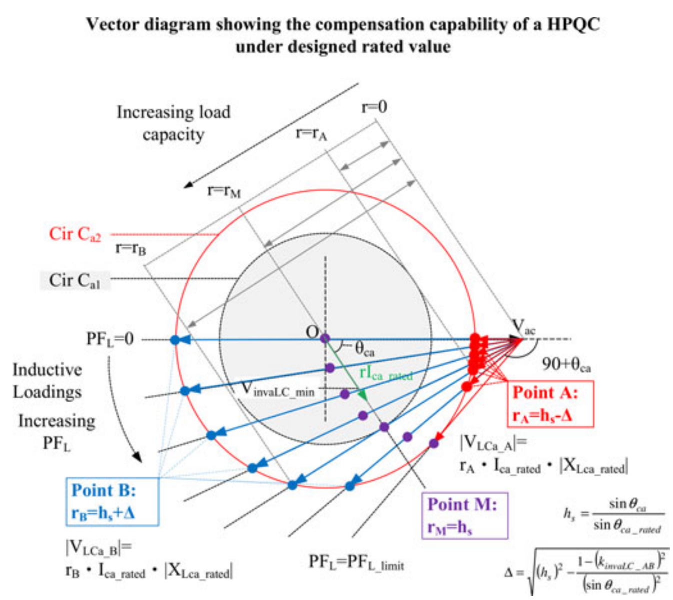

Fig. 9. Analysis of HPQC power quality compensation capability using vector diagram.

2) When the HPQC operation voltage rating is higher, the range of loading conditions that satisfactory compensation performance can be provided (compensation range) also gets larger.

3) The middle point r_M is located at $r = 1$ when ${\rm PF}_L = {\rm PF}_{\rm L\_rated}$; the value of r_M gets smaller when ${\rm PF}_L > {\rm PF}_{\rm L\_rated}$, and vice versa.

4) As load power factor ${\rm PF}_L$ increases, the compensation capability in terms of traction load capacity rating decreases.

$$k_{\rm invaLC\_AB} \ge \sqrt{\left(1 - r\cdot h_s\cdot(\sin\theta_{ca\_{\rm rated}})^2\right)^2 + (r\cdot h_c\cdot(\sin\theta_{ca\_{\rm rated}})\cdot(\cos\theta_{ca\_{\rm rated}}))^2} \tag{17}$$

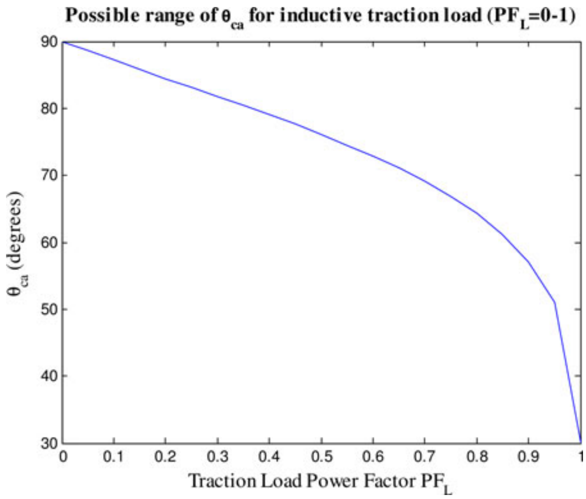

Fig. 10. MATLAB plot showing the possible range of V_{ac} phase compensation power angle θ_{ca} for inductive traction load ($PF = 0 - 1$) in cophase traction load.

D. Analysis of HPQC Compensation Capability Requirement When Load Varies

A vector diagram is shown in Fig. 9 for investigation of HPQC compensation capability when load varies. It is an extended version of the vector diagram in Fig. 7. It is still assumed that the HPQC is designed such that the minimum operation voltage is $V_{\mathrm{invaLC\_min}}$.

As discussed, the vector of HPQC operation voltage $V_{\mathrm{invaLC\_AB}}$ is determined by the vectors V_{ac} and $V_{\mathrm{LC}a}$. With fixed coupled impedance $X_{\mathrm{LC}a}$, the magnitude of vector $V_{\mathrm{LC}a}$ changes linearly with load capacity rating *r*. Furthermore, as load power factor changes, the direction of $V_{\mathrm{LC}a}$ also changes. Referring back to Fig. 9, when load power factor is zero, the vector $V_{\mathrm{LC}a}$ is in opposite direction of vector V_{ac}. As load power factor increases, the vector $V_{\mathrm{LC}a}$ rotates toward the lower half of the circle. The intersection points of the line extended from the vector $V_{\mathrm{LC}a}$ and the circle Cir C_{a2} then signify the boundary of the load conditions which HPQC can provide satisfactory compensation. Similarly, the point with lower load capacity is denoted as r_A, and that with high load capacity is denoted as r_B, which are points A and B in Fig. 8, with their expression in (18). The middle point of the loading condition is defined as r_M.

1) Variation of Load Power Factor PF_L*:* It is previously mentioned that as load power factor PF_L changes, the direction of vector $V_{\mathrm{LC}a}$ also changes. Notice that the direction of vector $V_{\mathrm{LC}a}$ is always 90° clockwise that of vector I_{ca}. Therefore, the angle between the vector V_{ac} and vector $V_{\mathrm{LC}a}$ is always $90^\circ + \theta_{\mathrm{ca}}$.

Traction locomotives are inductive loading, the possible range of θ_{ca} is presented using the curve in Fig. 10, which is constructed according to the expression in (7).

It can be observed from the figure that:

1) for cophase traction inductive loadings of power factor 0 to 1, the value of θ_{ca} ranges from 30° to 90°;
2) when load power factor increases, θ_{ca} decreases;
3) when the load power factor PF_L is zero, the vector $V_{\mathrm{LC}a}$ is parallel to the vector V_{ac}.

Furthermore, it can be observed from Fig. 9 that:

1) as load power factor $\mathrm{PF_L}$ increases, the vector V_{LCa} rotates toward the lower half of the circle Cir C_{a2} around the edge of vector V_{ac};
2) with a certain value of $V_{\mathrm{invaLC\_AB}}$, there is a boundary condition when $V_{\mathrm{LC}a}$ is tangent to the circle Cir C_{a2}; this is also the limit of load power factor variations, which will be discussed next.

As load power increases, the vector $V_{\mathrm{LC}a}$ rotates until a condition that the edge of $V_{\mathrm{LC}a}$ is located outside the HPQC compensation region. Under such condition, the HPQC cannot provide satisfactory compensation performance. This happens when there is no intersection point. In short, there is no rational solution of *r* for the expressions in (18). According to the mathematical theory, this refers to the conditions when Δ is not rational, which is shown as follows:

$$(h_s)^2 - \frac{1 - (k_{\mathrm{invaLC\_AB}})^2}{(\sin\theta_{ca\_\mathrm{rated}})^2} < 0. \tag{19}$$

By substituting the definition of h_s in (15) into (19), the expression in (20) can be obtained

$$\cos\theta_{ca} < k_{\mathrm{invaLC\_AB}}. \tag{20}$$

Therefore, the HPQC compensation capability is limited by (21). Referring back to the definition of θ_{ca} in (7), the power factor limit can then be determined as (22). It is interesting that the load power factor limit is not related to any rated value of the HPQC design, but is related to the HPQC operation voltage rating $k_{\mathrm{invaLC\_AB}}$ only

$$\theta_{ca\_\mathrm{limit}} = \cos^{-1}(k_{\mathrm{invaLC\_AB}}) \tag{21}$$

$$\mathrm{PF}_{L\_\mathrm{limit}} = \sqrt{\frac{4}{4 + \left[\tan\left(\cos^{-1}(k_{\mathrm{invaLC\_AB}})\right) - \frac{1}{\sqrt{3}}\right]^2}}. \tag{22}$$

The plot of HPQC operation voltage rating $k_{\mathrm{invaLC\_AB}}$ against power factor limitPFL_limit is shown in Fig. 11.

It is observed that as the HPQC operation voltage rating increases, the power factor limit also increases. For instance, with HPQC operation voltage rating of 0.66, the power factor limit is somewhere around 0.96. In other words, the HPQC cannot provide satisfactory compensation performance once the traction load power factor exceeds 0.96. The HPQC operation voltage may therefore also be chosen based on the desired load power factor limit.

2) Variation of Load Capacity Rating r: As introduced, the variation of load capacity is represented by the variation of r during analysis. When r increases, the amplitude of the vector $V_{\mathrm{LC}a}$ also increases toward the left-hand side of the circle Cir C_{a2} in Fig. 9. Under different load power factor PF_L, the intersection points r_A and r_B also vary according to (18), and Fig. 8. Notice that the middle point r_M is always located at h_s, which is the ratio of sin(θ_{ca}) to sin($\theta_{\mathrm{ca\_rated}}$);

1) when $\mathrm{PF}_L > \mathrm{PF}_{\mathrm{L\_rated}}, h_s < 1$, the middle point$\mathrm{r_M}$ is smaller than 1 p.u. (rated capacity);

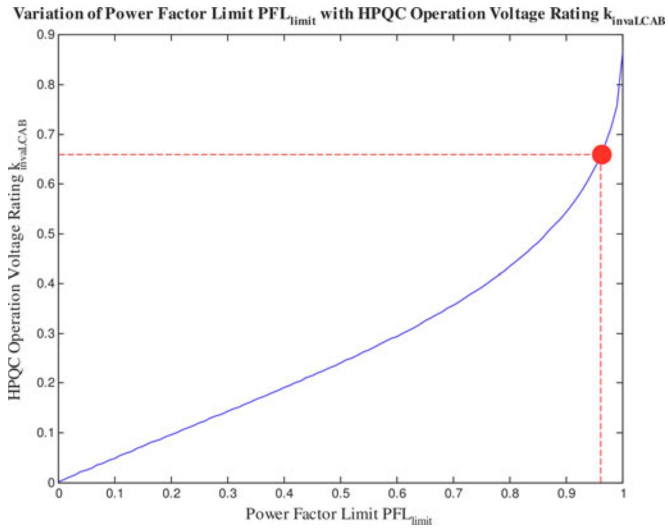

Fig. 11. MATLAB plot showing the variation of power factor limit $\mathrm{PF}_{L\_\mathrm{limit}}$ with HPQC Operation Voltage Rating $k_{\mathrm{invaLC\_AB}}$.

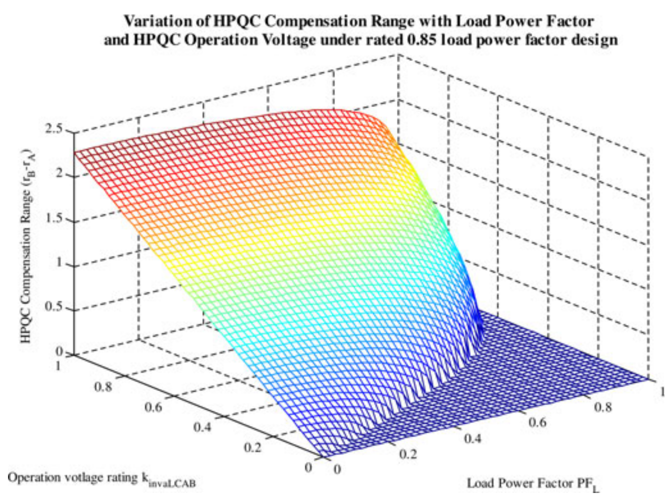

Fig. 12. Three-dimensional plot summarizing the variation of HPQC compensation range with load power factor and HPQC Operation Voltage under rated design of 0.85 load power factor.

2) when $\mathrm{PF}_L < \mathrm{PF}_{\mathrm{L\_rated}}, h_s > 1$, the middle point$\mathrm{r}_{\mathrm{M}}$ is greater than 1 p.u. (rated capacity).

This phenomenon can also be observed from the curves showing HPQC compensation capability in Fig. 8.

It is worth noticing that although the HPQC operation voltage is enhanced to increase compensation capability, the operation voltage is still less than conventional RPC, in which inductive coupled impedance is adopted and causes voltage drop across it during compensation.

E. Section Summary

The analysis of HPQC dc-link voltage and compensation capability within this section is summarized as follows.

1) Referring to Fig. 7, when HPQC is designed at minimum operation voltage under fixed rated load, it can only provide satisfactory at rated load condition and has minimum compensation capability.

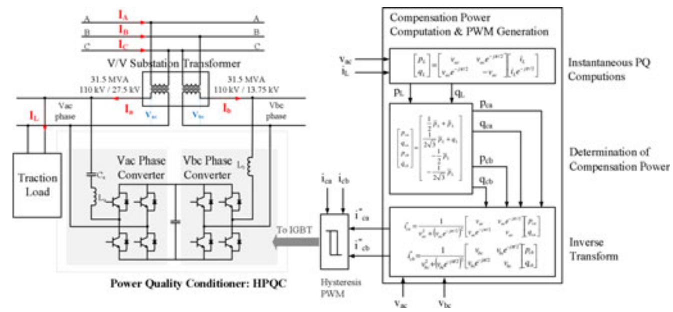

Fig. 13. Detailed circuit schematic and control of cophase traction power supply with newly proposed HPQC.

TABLE I
SYSTEM HPQC PARAMETERS USED IN SIMULATIONS OF COPHASE TRACTION POWER SUPPLY UNDER DIFFERENT LOAD CONDITIONS

Parameters	Descriptions	Value
V_{ac}	Load Voltage	27.5 kV
$\mathrm{I}_{\mathrm{ca\_rated}}$	V_{ac} phase compensation current	545 (A)
PF_{L}	Load Power Factor	0.85
θ_{ca}	V_{ac} phase compensation angle	61.28
$X_{\mathrm{LC}a\_\mathrm{rated}}$	V_{ac} coupled impedance	44.25
L_{a}	V_{ac} coupled inductance	2 (mH)
C_{a}	V_{ac} coupled capacitance	60 (uF)
L_{b}	V_{bc} coupled inductance	4 (mH)
$\mathrm{k}_{\mathrm{invaL}}$	RPC Operation Voltage Rating	0.66
V_{dc}	DC-Link Voltage	25.7 kV

2) When load varies in practical conditions, the HPQC operation voltage may need to be increased, the relationship between HPQC operation voltage and load condition variation range can then be determined by (18).

The expressions in (18) can be further investigated and summarized using Fig. 12, which is constructed based on rated load power factor value of 0.85. Referring to (7), (15), and (18), the HPQC compensation range $r_B - r_A$ is a function of HPQC operation voltage rating $k_{\mathrm{invaLC\_AB}}$ and load power factor PF_L. It can be observed from the diagram that:

1) the value of the compensation range r_{B}–r_{A} increases with increase in HPQC operation voltage;
2) when load power factor increases, the compensation range decreases;
3) there is a limit for load power factor limit, which is investigated in (22) and Fig. 11, the limit is dependent on $k_{\mathrm{invaLC\_AB}}$ only;
4) the load power factor limit increases with increase in HPQC operation voltage.

IV. SIMULATION AND EXPERIMENTAL VERIFICATIONS

In order to verify the relationship between HPQC DC operation voltage and its power quality compensation capability, PSCAD simulation verifications are performed to investigate the system performance under different loading conditions. A laboratory scaled hardware prototype is also constructed to obtain experimental results. The captured waveforms and data are shown next.

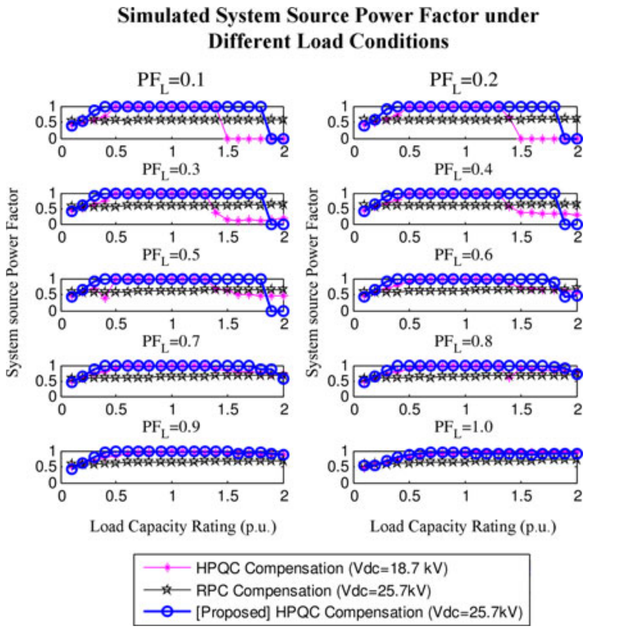

Fig. 14. Simulated system source power factor under different loading conditions, obtained from the cophase traction power with RPC and HPQC under various operation voltage.

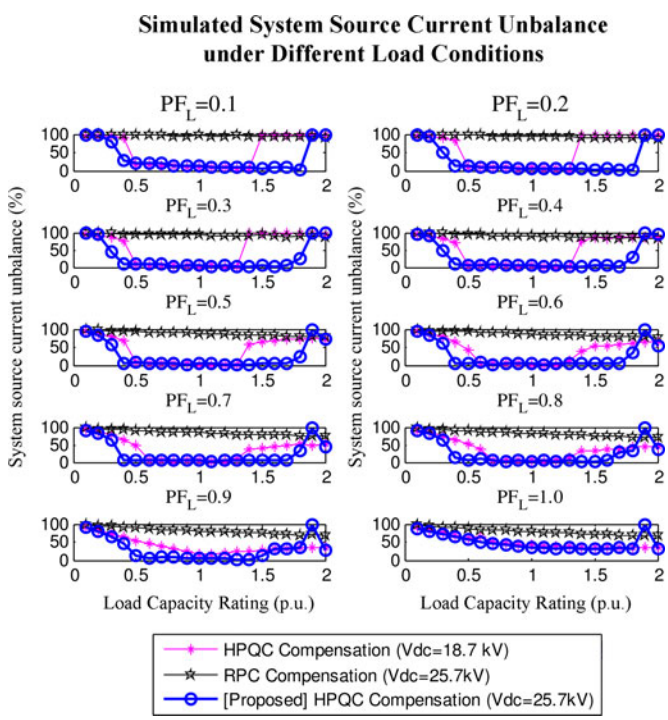

Fig. 15. Simulated system source current unbalance (%) under different loading conditions, obtained from the cophase traction power with RPC and HPQC under various operation voltage.

A. PSCAD Simulations

A detailed circuit schematic and control of cophase traction power with proposed HPQC in simulation verifications is shown in Fig. 13.

The parameter settings in the simulation are chosen based on common practical traction power supply system [6], [29].

TABLE II
BOUNDARY OF CALCULATED AND SIMULATED LOADING CONDITIONS WHICH HPQC CAN PROVIDE SATISFACTORY COMPENSATION PERFORMANCE WITH $k_{\mathrm{invaLC\_AB}} = 0.66$, $V_{\mathrm{DC}} = 25.7$ kV

PF_L	$h_s = r_M$	Calculated r_A	Calculated r_B	Simulated r_A	Simulated r_B
0.1	1.1401	0.3888	1.8914	0.4	1.8
0.2	1.1362	0.3908	1.8816	0.4	1.8
0.3	1.1298	0.3942	1.8653	0.4	1.8
0.4	1.1206	0.3992	1.8420	0.4	1.8
0.5	1.1080	0.4063	1.8097	0.4	1.8
0.6	1.0908	0.4166	1.7650	0.4	1.7
0.7	1.0663	0.4326	1.7001	0.4	1.6
0.8	1.0285	0.4607	1.5963	0.5	1.5
0.9	0.9584	0.5304	1.3865	0.6	1.4
1	0.5708	NA*	NA*	NA*	NA*

*NA: Not Available

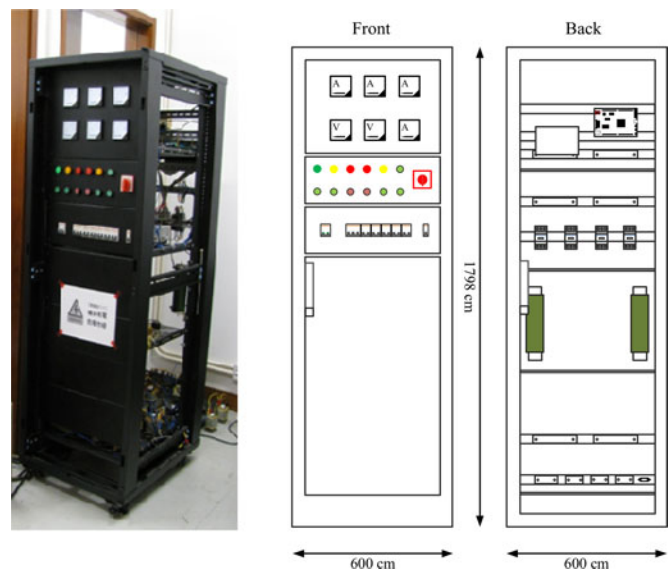

Fig. 16. Hardware appearance of a laboratory-scaled hardware prototype of cophase traction power supply with HPQC.

The three phase power grid is of 110 kV, 50 Hz and is transformed into two single phase outputs via V/V substation transformer. The V/V transformer is composed of two single phase transformers (31.5 MVA 110 kV/27.5 kV, 31.5 MVA 110 kV/13.75 kV), with V/V connections. One phase of substation output, V_{ac} phase, is connected to locomotive loadings, whereas another phase, V_{bc} phase, is unloaded. The power quality conditioner, HPQC, is then connected across the V_{ac} and V_{bc} phase in order to provide power quality compensation from secondary side to the three-phase primary source grid. Notice that the locomotive voltage is 27.5 kV, which is a bit higher than 25 kV, in order to compromise the voltage drop caused by inductive traction load.

The electronic switches used in the back-to-back converter of proposed HPQC are insulated-gate bipolar transistors (IGBT) for its high power application. The computation of required compensation power is accomplished according to (1) based on instantaneous *pq* theory. The compensation current reference is then obtained by performing inverse transform. The

TABLE III
PARAMETERS USED IN THE LABORATORY-SCALED HARDWARE PROTOTYPE OF COPHASE TRACTION POWER SUPPLY WITH HPQC

Parameters	Descriptions	Value
V_{ac}	Load Voltage	50 V
I_{ca_rated}	V_{ac} phase compensation current	2.65 (A)
PF_L	Load Power Factor	0.85
θ_{ca}	V_{ac} phase Compensation Angle	61.28
X_{LCa_rated}	V_{ac} coupled impedance	16.55
L_a	V_{ac} coupled inductance	2 (mH)
C_a	V_{ac} coupled capacitance	190 (uF)
L_b	V_{bc} coupled inductance	4 (mH)
k_{invaL}	RPC Operation Voltage Rating	0.66
V_{dc}	DC-Link Voltage	47 V

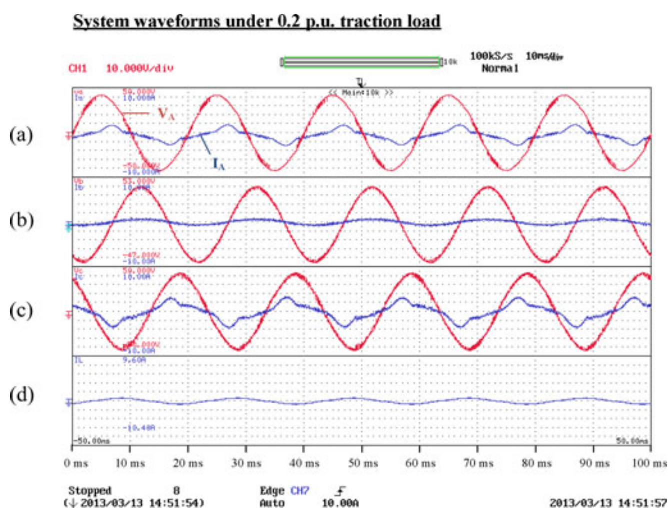

Fig. 17. Experimental system waveforms captured from the hardware prototype of cophase traction power with HPQC under load capacity 0.2 p.u. (a) phase A voltage and current; (b) phase B voltage and current; (c) phase C voltage and current; (d) load current.

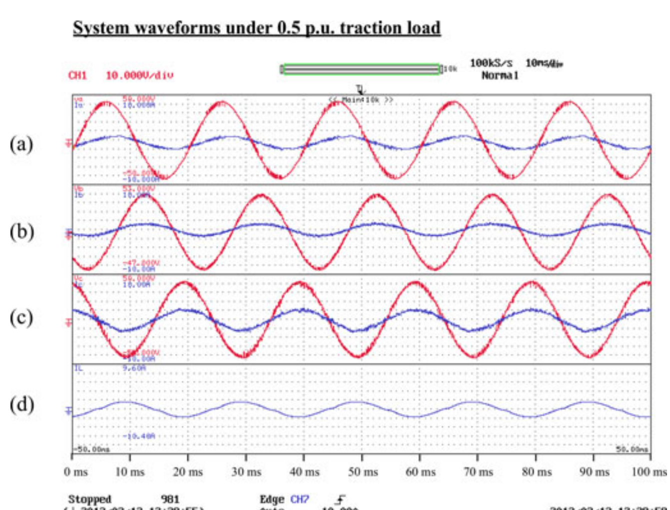

Fig. 18. Experimental system waveforms captured from the hardware prototype of cophase traction power with HPQC under load capacity 0.5 p.u. (a) phase A voltage and current; (b) phase B voltage and current; (c) phase C voltage and current; (d) load current.

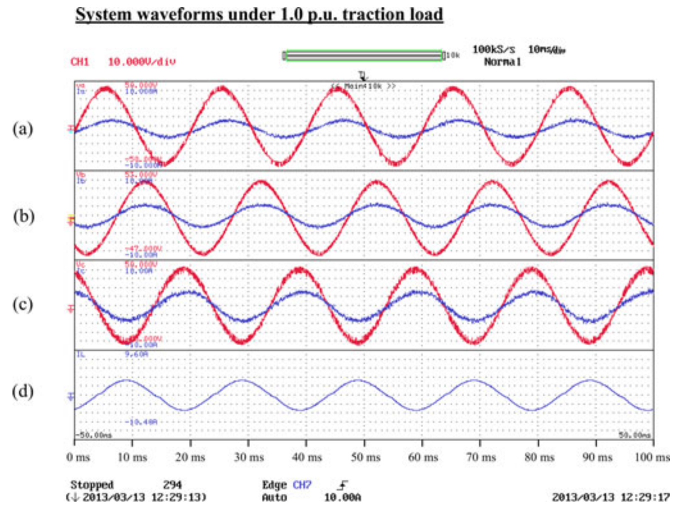

Fig. 19. Experimental system waveforms captured from the hardware prototype of cophase traction power with HPQC under load capacity 1.0 p.u. (a) phase A voltage and current; (b) phase B voltage and current; (c) phase C voltage and current; (d) load current.

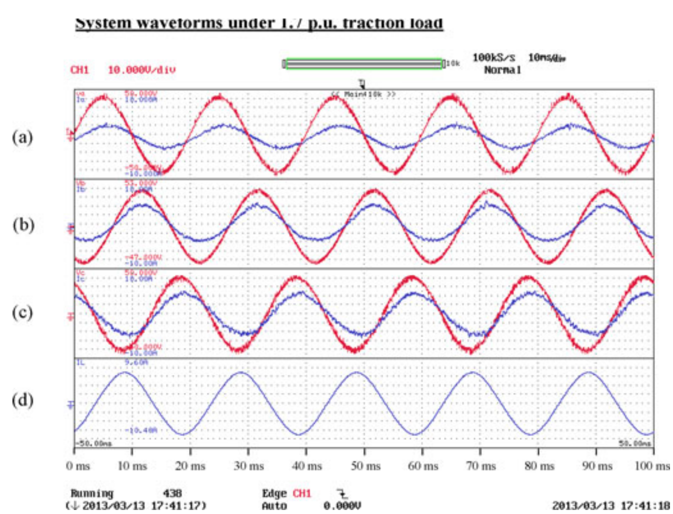

Fig. 20. Experimental system waveforms captured from the hardware prototype of cophase traction power with HPQC under load capacity 1.7 p.u. (a) phase A voltage and current; (b) phase B voltage and current; (c) phase C voltage and current; (d) load current.

compensation current reference is finally compared with the actual compensation current to generate pulse width modulation (PWM) signals for IGBT switches in Railway HPQC using linear-operated hysteresis PWM method in [30].

In the simulation, the HPQC control algorithm is completed according to (1) and is designed based on minimum operation voltage requirement at fixed rated load of power factor 0.85 and capacity 15 MVA (denoted as 1 p.u.). The traction load is then varied from 0.1 to 2 p.u. (0.1 p.u. step size), each with variation of load power factor 0 to 1 (0.1 step size).

The system parameters used in the simulation are shown in Table I. The V_{ac} phase coupled impedance is calculated using (6) and the coupled *LC* branch is designed at the fifth load harmonics.

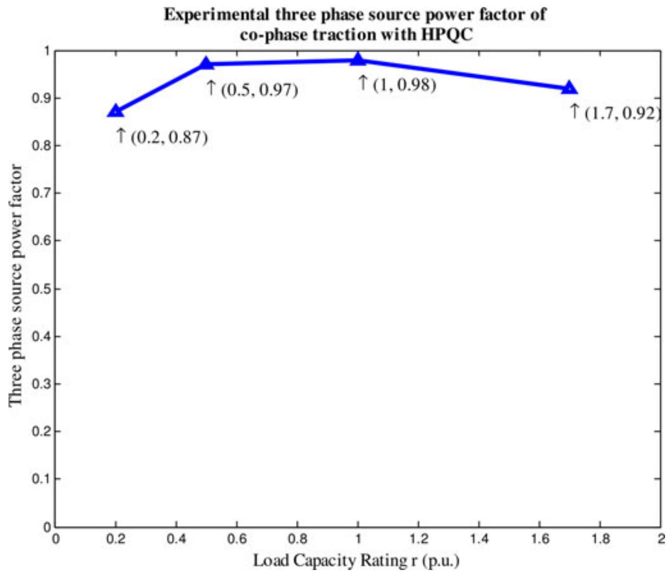

Fig. 21. Experimental system source power factor under four conditions 0.2, 0.5, 1.0, and 1.7 p.u.

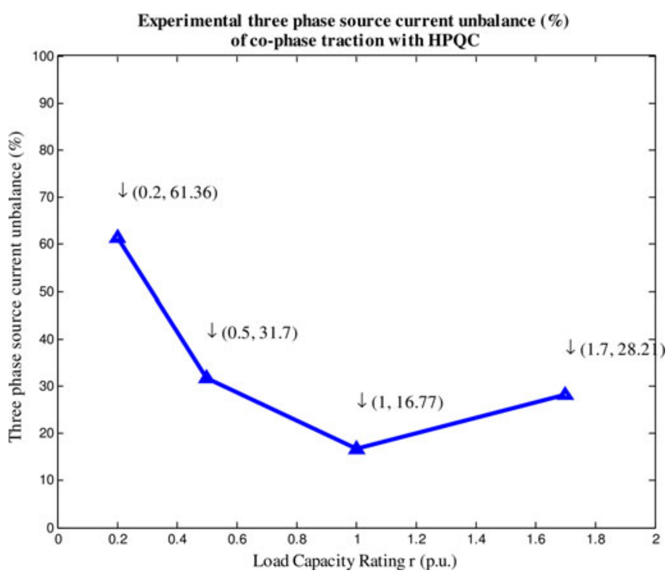

Fig. 22. Experimental system source current unbalance (%) under four conditions 0.2, 0.5, 1.0, and 1.7 p.u. traction load capacity.

As the condition in the analysis, the value of HPQC operation voltage rating $k_{\text{invaLC\_AB}}$ used is 0.66. The corresponding dc-link voltage is then 25.7 kV. The source power factor and current unbalance is being monitored.The simulated three-phase source power factor and current unbalance (%) under different load conditions obtained are shown in Figs. 14 and 15. Details of the statistics in the simulation can be found in appendix.

With satisfactory HPQC compensation, the source power factor is unity and the current unbalance is 0%. It can be observed from Figs. 14 and 15 that the HPQC can provide satisfactory compensation performance within a range of loadings.

As analyzed, the boundary of the range of loadings which HPQC can provide good compensation performance is defined by (18). The corresponding values of r_A, r_M and r_B calculated with $k_{\text{invaLC\_AB}} = 0.66$ under different load power factor PF_L are shown in Table II. The simulated values of r_A and r_B are also shown for comparisons. It can be observed that the simulated values are more or less the same as calculated ones. When $\text{PF}_L < \text{PF}_{\text{L\_rated}}$, the value of r_M is greater than 1.0 p.u.; on the other hand, when $\text{PF}_L > \text{PF}_{\text{L\_rated}}$, the value of r_M is smaller than 1.0 p.u.

The limit of load power factor in which HPQC can provide good compensation could also be investigated using (22). With $k_{\text{invaLC\_AB}} = 0.66$, the value of power factor limit $\text{PF}_{L\text{\_limit}}$ is 0.96.

In the simulation, when the load power factor is 1.0 (exceeding $\text{PF}_{L\text{\_limit}}$), the system source power factor and current unbalance is not satisfied.

For reference and comparison, the simulations are repeated using 1) conventional RPC with the same dc-link voltage at $k_{\text{invaL}} = 0.66$, $V_{\text{dc}} = 25.7$ kV; 2) HPQC with minimum dc-link voltage at rated design, $k_{\text{invaLC}} = 0.48$, $V_{\text{dc}} = 18.7$ kV [calculated using (8)]. The results are also presented in Figs. 14 and 15. It can be observed that consistent with the theoretical study, with conventional RPC operating at the same dc-link voltage, the system performance is far from satisfactory at any conditions. It could also be seen from the figures that the compensation capability is limited when using HPQC with operation voltage at its minimum value at rated load. The analysis of HPQC compensation capability is therefore verified via PSCAD simulations. They also show the significance of increasing HPQC operation voltage using proposed analysis in enhancing the compensation capability.

B. Experimental Results

A laboratory-scaled hardware of cophase traction power supply system with HPQC is constructed in order to obtain experimental verifications. The hardware appearance is shown in Fig. 16. It is constructed according to the circuit schematic in Fig. 12. The IGBTs within the HPQC are driven by IGBT drivers, and the PWM signals are generated based on the computation blocks shown in Fig. 12. The computation is achieved using DSP2812 (TDS2812EVMB), with ADC sampling frequency of 20 kHz. The rated load capacity is reduced from 15 MVA to 150 VA (ratio: 1:100k). Moreover, the load voltage is reduced from 27.5 kV to 50 V (ratio: 1:550).

The HPQC parameters are selected according to (6) at rated load capacity of 150 VA, with rated load power factor of 0.85. Detailed HPQC parameters can be found in Table III. With $k_{\text{invaLC\_AB}} = 0.66$, the dc-link voltage is 47 V.

With $k_{\text{invaLC\_AB}} = 0.66$, $\text{PF}_L = 0.85$, according to (18), the values of r_A and r_B are 0.49 and 1.51, respectively. Therefore, it is expected that satisfactory compensation performance can be provided within traction load capacity of 0.5 to 1.5 p.u. The system performance under four different cases are being investigated, namely 0.2, 0.5, 1.0, 1.7 p.u. The middle two conditions are inside the range, while the other two lies outside the range.

The system waveforms captured under the four investigated conditions are presented in Figs. 17 to 20. Detailed data of three phase source power factor and current unbalance can also be found in Figs. 21 and 22.

TABLE A1
SIMULATED THREE-PHASE SOURCE POWER FACTOR OF COPHASE TRACTION WITH HPQC ($V_{\rm DC} = 25.7$ KV)

	PF									
r	0.1	0.2	0.3	0.4	0.5	0.6	0.7	0.8	0.9	1
0.1	0.3811	0.3938	0.4065	0.4188	0.427	0.4316	0.438	0.4383	0.4351	0.5432
0.2	0.5265	0.5846	0.6017	0.6266	0.6479	0.6492	0.6519	0.6449	0.6295	0.549
0.3	0.8846	0.913	0.9216	0.9178	0.9206	0.9144	0.8821	0.8453	0.8056	0.686
0.4	0.9653	0.9987	0.993	0.9937	0.9975	0.9963	0.9967	0.984	0.9346	0.78
0.5	0.9983	0.9914	0.9964	0.9949	0.9872	0.9921	0.9959	0.998	0.9782	0.8528
0.6	0.9981	0.9935	0.9947	0.9969	0.997	0.9947	0.9968	0.9938	0.9949	0.908
0.7	0.9922	0.9906	0.9912	0.9949	0.9972	0.998	0.9985	0.9954	0.9927	0.9429
0.8	0.9979	0.9944	0.9994	0.9981	0.9971	0.9959	0.9939	0.9961	0.9896	0.9472
0.9	0.9934	0.9966	0.9961	0.9966	0.9991	0.997	0.9972	0.9966	0.9932	0.9388
1	0.9942	0.9981	0.9977	0.9968	0.9975	0.9981	0.9951	0.9986	0.9947	0.9303
1.1	0.994	0.9966	0.998	0.9971	0.9977	0.9971	0.9942	0.9942	0.9933	0.9259
1.2	0.9954	0.9968	0.9978	0.9963	0.9984	0.9973	0.9942	0.9959	0.9926	0.9158
1.3	0.9952	0.9978	0.9987	0.9982	0.9974	0.9953	0.9953	0.9954	0.9949	0.9096
1.4	0.9962	0.9991	0.9979	0.9983	0.9982	0.9965	0.9956	0.9963	0.9933	0.904
1.5	0.9976	0.9988	0.9989	0.9977	0.9985	0.9959	0.994	0.9972	0.9751	0.8995
1.6	0.9969	0.9968	0.9961	0.9963	0.9989	0.9962	0.9937	0.9927	0.9081	0.8543
1.7	0.9951	0.9997	0.9972	0.998	0.9967	0.9971	0.9934	0.9872	0.9543	0.9054
1.8	0.9987	0.9997	0.9948	0.9923	0.9921	0.8856	0.87	0.9517	0.9523	0.9061
1.9	0	0	0	0	0	0.4124	0.8572	0.8874	0.8961	0.9002
2	0	0	0	0	0	0.4458	0.573	0.716	0.8604	0.8929

It can be observed from the waveforms that for load capacity of 0.5 and 1.0 p.u., the system waveforms are satisfactory. The data points in Figs. 21 and 22 also reveal that under these conditions, the three-phase source power factor is near unity and with low current unbalance. These verify the satisfactory HPQC compensation performance and capability within the range.

On the other hand, for traction load capacity of 0.2 and 1.7 p.u., the system waveforms get distorted, and the phase angle between phase voltage and current also gets larger. It can also be seen from the data point in Figs. 21 and 22 that at load capacity of 0.2 and 1.7 p.u., the system source power factor and current unbalance gets worse. This indicates the unsatisfactory HPQC compensation performance at these load capacities (0.2 p.u., 1.7 p.u.).

Referring to the simulation results presented in Table II, Figs. 14, and 15, it can be observed that for load power factor of 0.8 and 0.9, with $k_{\rm invaLC} = 0.66$, the boundary of the range of loading capacity that satisfactory compensation can be provided are $r = [0.5, 1.5]$ and [0.6, 1.4], respectively.

V. CONCLUSION

In this paper, the relationship between HPQC dc-link voltage and its power quality compensation capability in cophase traction power is being analyzed and discussed. Cophase traction power has high potential to be power supply system. However, the operation voltage requirement of conventional inductive coupled RPC within the system is high due to its high power requirement to control power flow. This leads to higher cost and device ratings. The capacitive coupled HPQC is therefore newly proposed for reduction of operation voltage while providing similar performance at rated load. Nevertheless, reduction in HPQC operation voltage limits its power quality compensation capability. Therefore, it is essential to determine the relationship between HPQC dc operation voltage and the corresponding power quality compensation capability so as to provide a guideline for the design of HPQC.

It is found that when HPQC operates with minimum voltage under fixed rated load, the HPQC can only provide minimum compensation capability. Under practical conditions when load varies, the HPQC operation voltage may be enhanced so that HPQC can provide satisfactory compensation performance for a range of loading conditions. The boundaries of these conditions and limit are also investigated. The followings can be concluded from the analysis:

1) when HPQC dc-link voltage increases, the power quality compensation capability also gets larger;
2) when HPQC dc-link voltage increases over minimum value, the range of loading conditions which satisfactory compensation performance can be provided always include rated condition;
3) with a certain HPQC dc-link voltage, there is a upper limit of load power factor; when the load factor gets beyond this limit, HPQC cannot provide satisfactory compensation;
4) based on these, the HPQC dc-link operation voltage may be selected based on the loading conditions (possible range of load capacity rating and power factor).

Finally, PSCAD simulations are performed and experimental results are obtained from a laboratory-scaled hardware prototype to verify the analysis. The analysis provides a preliminary guideline for HPQC parameter selection when larger power quality compensation capability is preferred. For practical purpose, it would be preferable if the power quality compensation capability can be freely changed under a specific operation voltage and this worth further analysis and attention.

APPENDIX

Due to the page span, detailed data of simulation results in Section IV part A are presented in Tables A1 and A2 for readers' reference.

TABLE A2
SIMULATED THREE-PHASE SOURCE CURRENT UNBALANCE OF COPHASE TRACTION WITH HPQC (V_{DC} = 25.7 kV)

	PF									
r	0.1	0.2	0.3	0.4	0.5	0.6	0.7	0.8	0.9	1
0.1	98.28	97.19	96.51	94.8	94.34	93.31	92.12	91.52	90.5	88.12
0.2	98.61	93.83	92.47	88.8	85.14	84.29	82.42	80.99	79.38	81.32
0.3	78.05	51.53	45.2	50	57.6	61.86	63.12	64.39	66.05	70.89
0.4	28	13.38	9.76	8.37	5.47	4.76	5.44	11.97	45.65	63.6
0.5	18.88	12.46	8.61	7.56	9.68	7.19	4.27	3.99	13.96	56.62
0.6	19.9	10.89	9.68	5.7	4.11	7.53	5.01	8.11	5.53	50.65
0.7	19.42	10.74	8.63	7.82	4.82	3.48	4	4.33	7.88	45.12
0.8	13.67	10.09	3.81	3.95	6.2	5.37	7	3.81	9.34	41.51
0.9	14.15	6.96	6.43	3.96	2.91	4.07	4	4.81	7.02	38.75
1	11.46	5.21	4.57	7.15	4.63	4.33	7.37	0.99	4.05	36.08
1.1	10.56	4.98	3.09	2.2	3.93	2.49	2.64	6.08	6.15	34.22
1.2	8.32	6.55	4.9	5.1	1.75	4.75	5.84	3.02	6.37	32.97
1.3	8.91	5.13	2.57	2.45	3.51	6.31	4.34	5.38	2.97	34.09
1.4	8.09	4.86	2.13	3.72	1.95	4.41	5.12	3.66	2.67	31.78
1.5	6.12	2.52	4.05	4.46	4.7	5.01	5.42	2.59	12.8	30.8
1.6	9.29	5.36	2.12	5.27	4.76	4.25	4.28	6.9	29.78	33.07
1.7	7.83	2.94	4.298	1.11	4.89	4.61	5.12	28.12	30.5	33.9
1.8	3.47	2.41	24.51	28.52	25.71	34.26	32.05	34.54	35.12	31.51
1.9	99	99	99	99	99	99	99	99	99	99
2	99	99	99	94.58	73.26	54.26	44.57	36.68	26.13	32.14

REFERENCES

[1] P. Amrutha Paul, U. D. Anju, M. P. Anoop, M. Rajan Pallan, N. K. Roshna, and A. Sunny, "Effects of two phase traction loading on a three phase power transformer," in *Proc. Annu. Int. Conf. Emerg. Res. Areas, Magn., Mach. Drives*, 2014, pp. 1–5.

[2] V. P. Joseph and J. Thomas, "Power quality improvement of AC railway traction using railway static power conditioner a comparative study," in *Proc. Int. Conf. Power Signals Control Comput.*, 2014, pp. 1–6.

[3] N. Gunavardhini, M. Chandrasekaran, C. Sharmeela, and K. Manohar, "A case study on power quality issues in the Indian Railway traction sub-station," in *Proc. 7th Int. Conf. Intell. Syst. Control*, 2013, pp. 7–12.

[4] *IEEE Recommended Practice and Requirements for Harmonic Control in Electric Power Systems*, IEEE Std. 519-2014 (Revision of IEEE Std. 519-1992), 2014.

[5] *Quality of Electric Energy Supply Admissible Three Phase Voltage Unbalance*, National Standard GB/T 15543-2008, 2008.

[6] L. Battistelli, M. Pagano, and D. Proto, "2× 25-kV 50 Hz High-Speed traction power system: short-circuit modeling," *IEEE Trans. Power Del.*, vol. 26, no. 3, pp. 1459–1466, Jul. 2011.

[7] M. Chen, Q.-Z. Li, and G. Wei, "Optimized design and performance evaluation of new cophase traction power supply system" in *Proc. Power Energy Eng. Conf.*, 2009, pp. 1–6.

[8] Z. Shu, S. Xie, and Q.-Z. Li, "Development and implementation of a prototype for co-phase traction power supply system," in *Proc. Power Energy Eng. Conf.*, 2010, pp. 1–4.

[9] Q. Li, W. Liu, Z. Shu, S. Xie, and F. Zhou, "Co-phase power supply system for HSR," in *Proc. Int. Power Electron. Conf.*, 2014, pp. 1050–1053.

[10] Z. Shu, S. Xie, K. Lu, Y. Zhao, X. Nan, D. Qiu, F. Zhou, S. Gao, and Q. Li, "Digital detection, control, and distribution system for Co-Phase traction power supply application," *IEEE Trans. Ind. Electron.*, vol. 60, no. 5, pp. 1831–1839, May 2013

[11] S. W. Mohod and M. V. Aware, "A STATCOM-control scheme for grid connected wind energy system for power quality improvement," *IEEE Syst. J.*, vol. 4, no. 3, pp. 346–352, Sep. 2010.

[12] Y. Xiao, Y. H. Song, and Y.-Z. Sun, "Power flow control approach to power systems with embedded FACTS devices," *IEEE Trans. Power Syst.*, vol. 17, no. 4, pp. 943–950, Nov. 2002.

[13] H. F. Brown and R. L. Witzke, "Shunt capacitor installation for single phase railway service," *Trans. Am. Institute Electr. Eng.*, vol. 67, no. 1, pp. 258–266, 1948.

[14] R. Grünbaum, J. Hasler, and B. Thorvaldsson, "FACTS: Powerful means for dynamic load balancing and voltage support of AC traction feeders" in *Proc. IEEE Porto Power Tech*, 2001, vol. 4, pp. 1.

[15] G. Celli, F. Pilo, and S. B. Tennakoon, "Voltage regulation on 25 kV AC railway systems by using thyristor switched capacitor" in *Proc. 9th Int. Conf. Harmonics Quality Power*, 2000, vol. 2, pp. 633–638.

[16] A. Bueno, J. M. Aller, J. A. Restrepo, R. Harley, and T. G. Habetler, "Harmonic and unbalance compensation based on direct power control for electric railway systems," *IEEE Trans. Power Electron.*, vol. 28, no. 12, pp. 5823–5831, Dec. 2013.

[17] C. Wu, A. Luo, J. Shen, F. J. Ma, and S. Peng, "A negative sequence compensation method based on a two-phase three-wire converter for a high-speed railway traction power supply system," *IEEE Trans. Power Electron.*, vol. 27, no. 2, pp. 706–717, Feb. 2012.

[18] Z. Shu, S. Xie, and Q. Li, "Single-Phase Back-To-Back converter for active power balancing, reactive power compensation, and harmonic filtering in traction power system," *IEEE Trans. Power Electron.*, vol. 26, no. 2, pp. 334–343, Feb. 2011.

[19] Z. Sun, X. Jiang, D. Zhu, and G. Zhang, "A novel active power quality compensator topology for electrified railway," *IEEE Trans. Power Electron.*, vol. 19, no. 4, pp. 1036–1042, Jul. 2004.

[20] T. Besselmann, A. Mester, and D. Dujic, "Power electronic traction transformer: Efficiency improvements under light-load conditions," *IEEE Trans. Power Electron.*, vol. 29, no. 8, pp. 3971–3981, Aug. 2014.

[21] C. Zhao, D. Dujic, A. Mester, J. K. Steinke, M. Weiss, S. Lewdeni-Schmid, T. Chaudhuri, and P. Stefanutti, "Power electronic traction transformer—medium voltage prototype," *IEEE Trans. Ind. Electron.*, vol. 61, no. 7, pp. 3257–3269, Jul. 2014.

[22] D. Dujic, C. Zhao, A. Mester, J. K. Steinke, M. Weiss, S. Lewdeni-Schmid, T. Chaudhuri, and P. Stefanutti, "Power electronic traction transformer-low voltage prototype," *IEEE Trans. Power Electron.*, vol. 28, no. 12, pp. 5522–5534, Dec. 2013.

[23] N. Y. Dai, K. W. Lao, M. C. Wong, and C. K. Wong, "Hybrid power quality conditioner for co-phase power supply system in electrified railway," *IET Power Electron.*, vol. 5, no. 7, pp. 1084–1094, 2012.

[24] K.-W. Lao, N. Dai, W.-G. Liu, and M.-C. Wong, "Hybrid power quality compensator with minimum DC operation voltage design for high-speed traction power systems," *IEEE Trans. Power Electron.*, vol. 28, no. 4, pp. 2024–2036, Apr. 2013.

[25] K.-W. Lao, M.-C. Wong, N. Dai, C.-K. Wong, and C.-S. Lam, "A systematic approach to hybrid railway power conditioner design with harmonic compensation for high-speed railway," *IEEE Trans. Ind. Electron.*, vol. 62, no. 2, pp. 930–942, Feb. 2015.

[26] C.-S. Lam, M.-C. Wong, W.-H. Choi, X.-X. Cui, H.-M. Mei, and J.-Z. Liu, "Design and performance of an adaptive low dc voltage controlled LC-hybrid active power filter with a neutral inductor in three-phase four-wire power systems," *IEEE Trans. Ind. Electron.*, vol. 61, no, 6, pp. 2635–2647, Jun. 2014.

[27] W.-H. Choi, C.-S. Lam, M.-C. Wong, and Y.-D. Han, "Analysis of dc-link voltage controls in three-phase four-wire hybrid active power filters," *IEEE Trans. Power Electron.*, vol. 28, no. 5, pp. 2180–2191, May 2013.
[28] J. Ma, M. Wu, and S. Yang, "The application of SVC for the power quality control of electric railways," in *Proc. Int. Conf. Sustainable Power Gener. Supply*, 2009, pp. 1–5.
[29] K. Yu, *Electric Railway Power Supply and Power Quality*, Beijing, China: China Electric Power Press, 2010.
[30] C.-S. Lam, M.-C. Wong, and Y.-D. Han, "Hysteresis current control of hybrid active power filters," *IET Power Electron.*, vol. 5, no. 7, pp. 1175–1187, Aug. 2012.

Keng-Weng Lao (S'09) was born in Macau, China, in 1987. He received the B.Sc. and Master degrees in electrical and electronics engineering from the Faculty of Science and Technology, University of Macau, Macao, China, in 2009 and 2011, respectively. He is currently working toward the Ph.D. degree at the Department of Electrical and Computer Engineering, University of Macau.

His research interests include FACTS compensation devices, energy saving, and renewable energy.

Mr. Lao was the first runner-up of the Challenge Cup National Inter-varsity Science and Technology Competition, and Championship of the Postgraduate Section in the IET Young Professionals Exhibition & Competition in China and Hong Kong, respectively, in 2013. He also received the Champion Award of the Schneider Electric Energy Efficiency Cup in Hong Kong in 2010.

Man-Chung Wong (SM'06) received the B.Sc. and M.Sc degrees in electrical and electronics engineering from the Faculty of Science and Technology, University of Macau, Macao, China, in 1993 and 1997, respectively, and the Ph.D degree from Tsinghua University, Beijing, China, in 2003.

He has been an Associate Professor at the University of Macau since 2008. His research interests include FACTS and DFACTS, power quality, custom power, and PWM.

Dr. Wong received the Young Scientist Award from the "Instituto Internacional De Macau" in 2000, the Young Scholar Award from the University of Macau in 2001, second prize of 2003 Tsinghua University Excellent Ph.D thesis Award, and third prize of 2012 Macao Technology Invention Award given by the Macao Science and Technology Fund (FDCT).

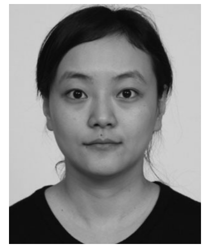

Ning Yi Dai (S'05–M' 08) was born in Jiangsu, China, in 1979. She received the B.Sc. degree in electrical engineering from Southeast University, Nanjing, China, in 2001, and the M.Sc. and Ph.D. degrees in electrical and electronics engineering from the Faculty of Science and Technology, University of Macau, Macao, China, in 2004 and 2007, respectively.

She is currently an Assistant Professor in the Department of Electrical and Computer Engineering, University of Macau. She has published more than 30 technical journals and conference papers in the field of power system and power electronics. Her research interests include application of power electronics in power system, renewable energy integration, and pulse width modulation.

Chi-Kong Wong (M'91) was born in Macao in 1968. He received the B.Sc. and M.Sc. degrees in electrical and electronics engineering (EEE) at the University of Macau, Macao, China, in 1993 and 1997, respectively, and the Ph.D. degree in EEE from Tisnghua University, Beijing, China, in 2007.

He has been with the University of Macau as a Teaching Assistant for the Faculty of Science and Technology since 1993 and became a Lecturer and an Assistant Professor in 1997 and 2008, respectively. Since 1997, he has been teaching the fundamental courses for the Department of Electrical and Electronics Engineering and supervising the final year projects. In addition of the undergraduated teaching and supervision, he had also cotaught one master course and cosupervised three master research projects. From 1997 to 2007, he had conducted four University research projects and five external projects from CEM and organized one power system protection training course to CEM staffs. His research interests include voltage stability analysis, synchronized phasor measurement applications in power systems, wavelet transformation applications in power systems, renewable energy, and energy saving.

Chi-Seng Lam (S'04–M'12) received the B.Sc., M.Sc., and Ph.D. degrees in electrical and electronics engineering from the University of Macau (UM), Macao, China, in 2003, 2006, and 2012, respectively. He is currently working toward the Ph.D. degree from Power Electronics Laboratory, UM.

From 2006 to 2009, he was an Electrical and Mechanical Engineer in the Campus Development and Engineering Section, UM. In 2009, he returned to the Power Electronics Laboratory of UM to work as a Technician. In 2013, he was a Postdoctoral Fellow in The Hong Kong Polytechnic University, Hong Kong, China. He is currently an Assistant Professor in the State Key Laboratory of Analog and Mixed-Signal VLSI, UM, Macao, China. He has coauthored one book: Design and Control of Hybrid Active Power Filters (New York, NY, USA: Springer, 2014), two Chinese patents, and more than 30 technical journals and conference papers. His research interests include integrated power electronics controller, power management IC design, power quality compensators, electric vehicle charger and renewable energy.

Dr. Lam received the Macao Science and Technology Invention Award (Third-Class) in 2014. He also received the Macao Science and Technology R&D Award for Postgraduates (Ph.D. Level) in 2012 and the third Regional Inter-University Postgraduate Electrical and Electronic Engineering Conference Merit Paper Award in 2005. In 2007 and 2008, he was the GOLD Officer and Student Branch Officer of IEEE Macau Section. He is currently the Secretary of IEEE Macau Section and IEEE Macau PES/PELS Joint Chapter.